STDP-based Unsupervised Learning of Memristive Spiking Neural Network by Morris-Lecar Model

Amirali Amirsoleimani, Majid Ahmadi and Arash Ahmadi
Research Center for Integrated Microsystems
University of Windsor
Windsor, Ontario, Canada
Email: {amirsol, ahmadi, aahmadi}@uwindsor.ca

***Abstract*—These days, there is an increasing interest in implementation of spiking neural systems that can be used to perform complex computations or solve pattern recognition tasks like mammalian neocortex. In this paper, Morris-Lecar neuron neuron is utilized to implement bio-inspired memristive spiking neural network for unsupervised learning applications. The spike timing dependent plasticity learning mechanism has been applied as the learning scheme in the system. The memristive implementation of the Morris-Lecar neuron has been analyzed. Also the memristors are utilized as the synapses for the proposed system to reproduce long term potentiation and long term depression. The proposed platform is tested for pattern classification applications and the results are successfully confirmed its functionality.**

***Keywords*—Memristor, Morris-Lecar, Spike-Timing-Dependent-Plasticity (STDP), Spiking Neural Network (SNN), Learning, Neuron.**

I. Introduction

Spiking Neural Network (SNN) is a promising generation of Artificial Neural Network (ANN) that can be comparable in terms of efficiency in processing information to its biological counterparts [1]. Today, this may be a lost part of the hardware puzzle due to the growing needs for high volume data processing in the coming era of bioinformatics [2]. In SNN, the presence and timing of individual spikes are considered as the main scheme for communication and neural computation [3]. Pulse-coupled neural networks with spike-timing are considered as a vital component in biological information processing systems, such as the brain. Understanding brain function, as one of the most attractive topics in neuroscience, can lead to discovery of new bio-inspired computing systems. Hence, it is crucial to model biological mechanism in brain specifically for the neurons and synapse to have a deeper understanding of brain information processing mechanisms.

In recent years, several different neuron models have been presented [4-9]. These models can be categorized into conductance-based models [4-7] with biological precision and spiking-based models [8-9], that describe temporal behavior of cortical spike train. Hudgkin-Huxley [4] is the pioneer of conductance-based model to describe the physiological mechanisms of neuronal behavior in central nervous system. Despite its high accuracy in defining a biological behavior of the neuron, it has a high computational cost for implementation due to its complexity. Thus, selecting a simpler model, which has a lower complexity and acceptable accuracy, is a viable alternative for low cost hardware implementation of bio-inspired neural systems.

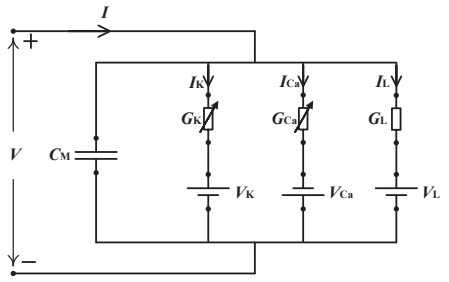

Fig. 1. Equivalent circuit schematic for ML neuron model.

Morris-Lecar (ML) model [7] is one of the computationally efficient conductance-based neuron models that offers a reasonable accuracy to produce biophysical behavior of neuronal activities. This model was developed to define the dynamics of the barnacle muscle fiber. The ML model includes a set of first order differential equations that reproduce the evolution of the membrane potential, calcium current and potassium current. Interestingly, ML neuron potassium and calcium current equations show memristive behavior [10]. Thus, ML neurons can be implemented by utilizing the nanoscale memristors which reduces the area overhead for hardware implementation ML-based neural systems significantly.

Memristor is an analog memory device, which can be fabricated in high density nano-scale fabrics. Unique characteristics of this new emerging technology has shown a great potential to be used as biological synaptic connection in bio-mimic hardware [11]. In addition, it can reproduce Spike-Timing-Dependent-Plasticity (STDP). Memristor crossbar architecture opens the opportunity to have ultra size scaling of very large scale neural networks. Recently, several studies have been done on neuromorphic computing with memristor devices but most of them employed spiking-based neuron model like Integrate and Fire (IF) and Leaky Integrate and Fire (LIF) [12]. Memristive neuromorphic computing using biological plausible model of neuron [19] is worth to be implemented as it leads to understanding of real neuronal interactions in brain.

In this paper, unsupervised STDP-based learning is tested for memristive SNN by utilizing ML neuron. The memristive implementation of the ML neuron is analyzed by showing the potassium and the calcium channels memristive behavior. The coupled ML neurons behavior by using a memristive synapse are assessed for STDP learning rule. For testing

978-1-5090-6182-2/17/$31.00 ©2017 IEEE

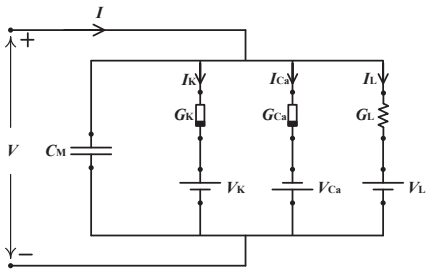

Fig. 2. Equivalent memristive circuit schematic for ML neuron model.

the functionality of proposed SNN, two pattern classification applications are implemented by this scheme. The results of the simulations for pattern classifications are presented. Rest of this paper is organized as follows. The definition of memristor, its functionality and its model are defined in section II. In section III, Morris-Lecar neuron and its memristive implementation is explained. The memristor synapse and STDP learning mechanism are defined in section IV. The proposed SNN structure and its behavior are described in Section V. In section VI the pattern classification results and outputs are presented. Finally in section VII conclusion and remarks are provided.

II. Memristor Device and Its Functionality

A nanoscaled passive two-terminal resistive device with non-volatile characteristics was discovered in 2008 by researchers in HP lab [13]. This device had been envisioned earlier in 1971 by Leon Chua [14]. The pinched hysteresis $i-v$ curve of memristor represents its unique memory-dependent feature. These devices have been utilized in various applications such as, nanoelectronic memories [15], logic implementation [16-17] and neuromorphic [18-19]. Memristor comprises of an electrically switchable thin film sandwiched between two metal contacts with a total length of L. The thin film consists of doped and undoped regions. The instantaneous voltage and current of memristor device obey a state-dependent Ohm's law. The voltage-controlled device can be defined by,

$$i = G(v,w,t)v, \tag{1}$$

$$\frac{dw}{dt} = f(v,w,t)v. \tag{2}$$

The length of doped region, w, is considered as the internal state variable of the device. By applying a voltage higher than positive $(V_{\rm tp})$ and negative $(V_{\rm tn})$ threshold of the device, the internal state variable is altered and the device resistance is changed between low resistance state $(R_{\rm LRS})$ and high resistance state $(R_{\rm HRS})$.

III. Morris-Lecar Neuron

The ML model [7] was developed to generate the biological behavior of calcium Ca^{++} and potassium K^{++} conductances in giant barnacle muscle fiber. This model has three ionic currents: a membrane leakage current, a potassium current and a calcium current. The electrical equivalent circuit for this model is defined in Fig. 1. The simplest form of the ML model is defined by,

$$I = C_{\rm M}\frac{dV}{dt} + I_{\rm ionic}. \tag{3}$$

$$I_{\rm ionic} = I_{\rm Ca} + I_{\rm K} + I_{\rm L}, \tag{4}$$

where I, V and $C_{\rm M}$ are the total membrane current, voltage and capacitance, respectively. The ionic current, $I_{\rm ionic}$, consists of calcium $(I_{\rm Ca})$, potassium $(I_{\rm K})$ and leakage $(I_{\rm L})$ currents. These three currents are determined by,

$$I_{\rm Ca} = g_{\rm Ca}M\left(V\right)\left(V - V_{\rm Ca}\right), \tag{5}$$

$$I_{\rm K} = g_{\rm K}N(V - V_{\rm K}), \tag{6}$$

$$I_{\rm L} = g_{\rm L}(V - V_{\rm L}), \tag{7}$$

where $g_{\rm Ca}$, $g_{\rm K}$ and $g_{\rm L}$ are maximum or instantaneous conductance for calcium, potassium and leakage channels, respectively. The parameters $V_{\rm Ca}$, $V_{\rm K}$ and $V_{\rm L}$ are equilibrium potentials corresponding to calcium, potassium and leakage channels, respectively. M and N denote the fraction of open calcium and potassium channels, respectively. These parameters can be determined by,

$$\frac{dM}{dt} = \lambda_{\rm M}(V)\left[M_\infty(V) - M\right], \tag{8}$$

$$M_\infty\left(V\right) = 0.5\left\{1 + \tanh\left(\frac{V - V_1}{V_2}\right)\right\}, \tag{9}$$

$$\lambda_{\rm M}(V) = \bar{\lambda}_{\rm M}(V)\cosh\left[\frac{V - V_1}{2V_2}\right], \tag{10}$$

$$\frac{dN}{dt} = \lambda_{\rm N}(V)\left[N_\infty(V) - N\right], \tag{11}$$

$$N_\infty\left(V\right) = 0.5\left\{1 + \tanh\left(\frac{V - V_3}{V_4}\right)\right\}, \tag{12}$$

$$\lambda_{\rm N}(V) = \bar{\lambda}_{\rm N}(V)\cosh\left[\frac{V - V_3}{2V_4}\right], \tag{13}$$

where M_∞ and N_∞ denote the fraction of open calcium and potassium channels at steady state, respectively. The parameter V_1 and V_3 are the membrane potential value at $M_\infty = 0.5\mathrm{mV}$ and $N_\infty = 0.5\mathrm{mV}$, respectively. V_2 and V_4 are reciprocal of slope of voltage dependent M_∞ and N_∞, respectively. The parameters $\lambda_{\rm M}(\mathrm{V})$ and $\lambda_{\rm N}(\mathrm{V})$ are rate constants for opening of calcium and potassium channels, respectively. In addition, the maximum rate constants for opening of calcium and potassium channels are $\bar{\lambda}_{\rm M}(V)$ and $\bar{\lambda}_{\rm N}(V)$, respectively. By assuming that the response of the calcium ion is considerably faster than the response of the potassium ion and the state equation of calcium is in the steady state, $\frac{dM}{dt} = 0$ $(M = M_\infty(V))$, the differential equation in (1) is simplified to second-order form as follows,

$$C_{\rm M}\frac{dV}{dt} = -g_{Ca}M_\infty(V)\left[V - V_{Ca}\right] - g_K N(V)\left[V - V_K\right] - g_L\left[V - V_L\right] + I \tag{14}$$

By analyzing the general form of the ML model, it can be deduced that the calcium and potassium channels are showing memristive behavior [10]. The time-varying conductance in potassium and calcium channels can be defined by two memristors as it is displayed in Fig. 2. The parameters N and M are similar to the state variable of memristor devices. By simulating the current in potassium and calcium channels a pinched hysteresis loop under bipolar periodic signal is extracted. This feature is similar to the unique characteristic of memristor

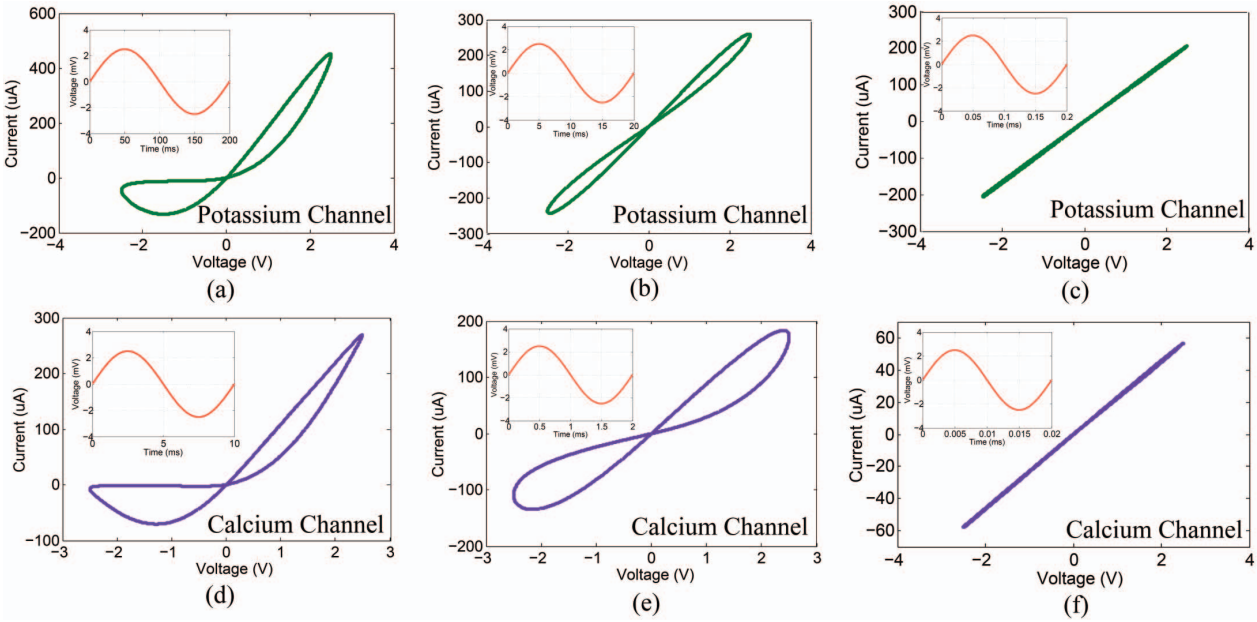

Fig. 3. Memristive behavior of potassium and calcium channels for ML model is displayed for $2.5V$ sinusoidal voltage input wave in different frequencies. (a) Potassium channel memristor $i-v$ for 5 Hz. (b) Potassium channel memristor $i-v$ for 50 Hz. (c) Potassium channel memristor $i-v$ for 5 KHz. (d) Calcium channel memristor $i-v$ for 100 Hz. (e) Calcium channel memristor $i-v$ for 500 Hz. (f) Calcium channel memristor $i-v$ for 50 KHz.

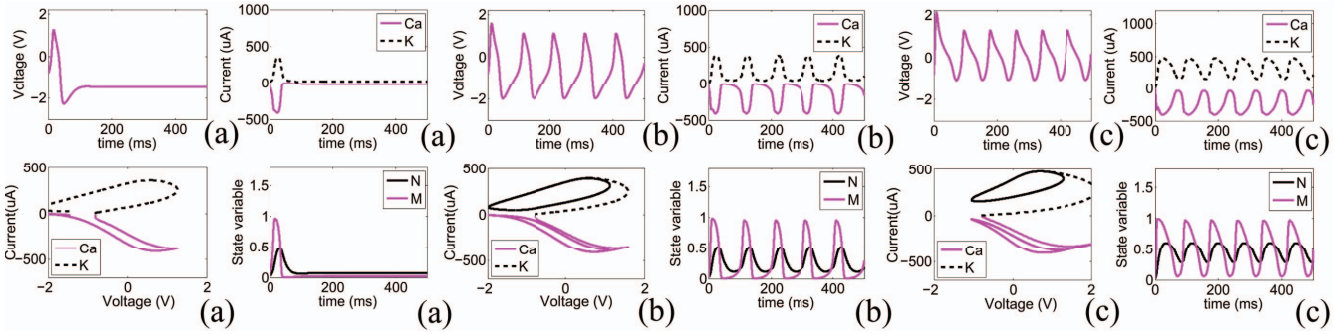

Fig. 4. The scaled ML neuron bifurcation behavior for different current stimulus. The membrane voltage, calcium channel's current, potassium channel's current and state variables (M, N) are analyzed in each case. (a) The stimulus current of 60 μA. (b) The stimulus current of 100 μA. (c) The stimulus current of 200 μA.

TABLE I. SCALED MORRIS-LECAR NEURON PARAMETERS.

Parameters	Value	Parameters	Value	Parameters	Value
$g_{\mathrm{Ca}}(\mu\mathrm{Scm}^{-2})$	0.11	$V_{\mathrm{CA}}(\mathrm{V})$	4.8	$C_{\mathrm{M}}(\mu\mathrm{Fcm}^{-2})$	0.5
$g_{\mathrm{K}}(\mu\mathrm{Scm}^{-2})$	0.2	$V_{\mathrm{K}}(\mathrm{V})$	-3.36	$\bar{\lambda}_{\mathrm{N}}(\mathrm{ms}^{-1})$	40
$g_{\mathrm{L}}(\mu\mathrm{Scm}^{-2})$	0.05	$V_{\mathrm{L}}(\mathrm{V})$	-2.4	$\bar{\lambda}_{\mathrm{M}}(\mathrm{ms}^{-1})$	800

devices. In addition, by increasing the frequency of the applied bipolar periodic signal, the hysteresis loops are shrunk and by reaching to a specific frequency it becomes to a single-value function through the origin. Hence, these properties prove the memristive nature of calcium and potassium channels in ML model. The memristive equivalent model for ML is depicted in Fig. 2. For utilizing the ML model in the proposed SNN, the ML model is scaled to around 2V. The parameters for scaled ML model are defined in Table 1. The $i-v$ curve of the potassium and calcium channels are displayed in Fig. 3 for different frequencies. In addition, the bifurcation and parameters behavior in the proposed scaled ML neuron are illustrated in Fig. 4 for three different applied currents to the neuron.

IV. STDP LEARNING MECHANISM WITH MEMRISTOR SYNAPSES

STDP is a timing-based learning mechanism postulated to exist in biological neurons of mammalian neocortex [18]. The functionality of this mechanism is based on the relative timing of spikes arrival from pre-synaptic and post-synaptic neurons. Long term potentiation (LTP) and long term depression (LTD) phenomenons can be generated by STDP mechanism and they cause alteration in synaptic efficacy (weight). LTP happens when pre-synaptic neuron spike proceeds the post-synaptic neuron ($t_{\mathrm{post}} - t_{\mathrm{pre}} \geq 0$) and it increases the synaptic weight (W). LTD takes place when post-synaptic synaptic neuron spikes before pre-synaptic neuron ($t_{\mathrm{post}} - t_{\mathrm{pre}} < 0$) and this results in reduction of synaptic weight. The degree of change in

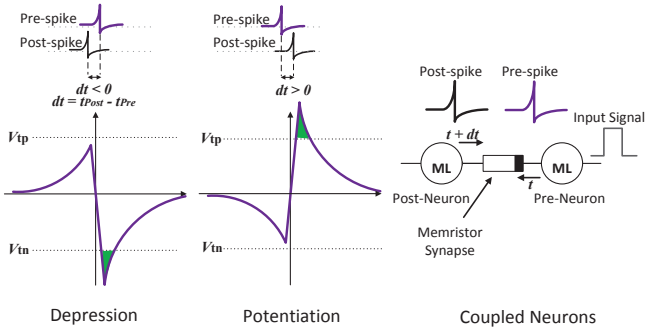

Fig. 5. STDP learning mechanism is illustrated for two coupled ML neurons with a memristive synapse. LTD and LTP phenomenons are displayed.

synaptic weight is a function of the time interval between post- and pre-synaptic spikes. The larger changes are induced by shorter time interval. Interestingly, the memristor device behavior mimics biological synapse in the brain as its conductance can be modulated by applying a stimuli with an ability to store the information [11]. These devices are capable of reproducing STDP mechanism similar to biology. In LTP phenomenon, the voltage over the memristor synapse becomes greater than positive threshold of the device ($V_{\rm post} - V_{\rm pre} \geq V_{\rm tp}$) and the conductance (weight) of the memristor increases. On the other hand, in LTD phenomenon the voltage over the memristor synapse becomes less than negative threshold of the device ($V_{\rm post} - V_{\rm pre} < V_{\rm tn}$) and it results a reduction in conductance (weight) of the memristor. The STDP learning mechanism is displayed for proposed SNN with memristive synapse in Fig. 5.

V. The Memristive SNN with ML Neuron

The architecture of the proposed SNN comprises of ML neurons and voltage-controlled memristor synapses. The scaled ML model, with parameters presented in Table 1, generates biological plausible shape of spike. The memristor model [20] is applied for memristor synapse and its parameters are defined in Table 2. The proposed SNN has a pre-synaptic neurons layer that is connected with memristive synapses to post-synaptic neurons layer. To analyze the behavior of the SNN, at first two coupled ML neurons with one memristive synapse is assessed. The pre-synaptic neuron's membrane voltage can be determined by,

$$C_{\rm M}\frac{dV_{\rm pre}}{dt} = -g_{\rm Ca}M_{\infty}(V_{\rm pre})\left[V_{\rm pre} - V_{Ca}\right] - g_K N(V_{\rm pre})\left[V_{\rm pre} - V_K\right] - g_L\left[V_{\rm pre} - V_L\right] + I. \quad (15)$$

The parameter $V_{\rm pre}$ is pre-synaptic neuron's membrane voltage. The parameter I is the applied input current to pre-synaptic neuron. The applied current to pre-synaptic neurons for proposed SNN is considered 100 μA which produces hopf bifurcation in ML neuron model. The membrane voltage of the post-synaptic neuron can be determined by,

$$C_{\rm M}\frac{dV_{\rm post}}{dt} = -g_{\rm Ca}M_{\infty}(V_{\rm post})\left[V_{\rm post} - V_{Ca}\right] - g_K N(V_{\rm post})\left[V_{\rm post} - V_K\right] - g_L\left[V_{\rm post} - V_L\right] + I_{\rm syn}. \quad (16)$$

The parameter $V_{\rm post}$ is membrane voltage of the post-synaptic neuron. The $I_{\rm syn}$ is the total current enters the post-synaptic neuron by memristive synapses and in this case it is equal to the current passes memristor synapse. In larger SNN, as post-synaptic neuron is connected to k pre-synaptic neurons with memristive synapses that have currents ($I_{\rm syn1}$,$I_{\rm syn2}$,...,$I_{{\rm syn}k}$), the pre-synaptic neuron current is equivalent to,

$$I_{\rm syn} = \sum_{j=1}^{k} I_{{\rm syn}j}. \quad (17)$$

The synaptic current in each synapse varying due to the conductance change happens in each synapse during neuronal activities. As the voltage over each synapse exceeds the positive and negative threshold of the device, the LTP and LTD phenomenons occur and the conductance of the synapses alter. The current of each synapse $I_{{\rm syn}j}$ can be determined as,

$$I_{{\rm syn}j}(t) = \frac{V_{\rm post}(t) - V_{{\rm pre}j}(t)}{R_{{\rm syn}j}(wj)}, \quad (18)$$

$$R_{{\rm syn}j}(w_j) = R_{\rm LRS}\frac{w_j(t)}{L} + R_{\rm HRS}(1 - \frac{w_j(t)}{L}), \quad (19)$$

$$\frac{dw_j}{dt} = \frac{\mu_v R_{\rm LRS}}{L^2} \times I_{{\rm syn}j}(t) \times f(w_j), \quad (20)$$

$$f(w_j) = \left(1 - 2\left(\frac{w_j(t)}{L}\right)\right)^{2p}. \quad (21)$$

The parameter $f(w_j)$ is the window function [20] for each synapse and p is a constant. The p value is considered 2 in simulations. The pattern classification application has been tested for the proposed SNN.

TABLE II. Memristor Device Parameters for Simulation.

Parameters	$R_{\rm LRS}$	$R_{\rm HRS}$	L	μ_v	$V_{\rm tp}$	$V_{\rm tn}$
Units	Ω	KΩ	nm	m^2/Vs	V	V
Values	100	10	3	1×10^{-15}	1.5	-1.2

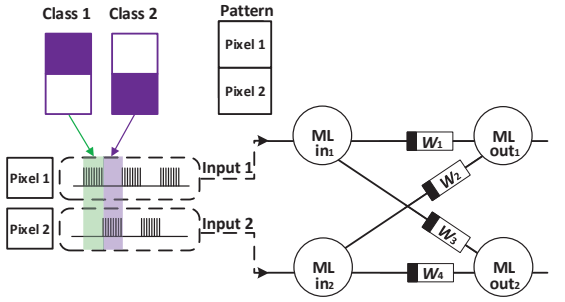

Fig. 6. 2×2 network architecture of the proposed SNN. The input patterns for the proposed network are defined.

VI. Pattern Classification Results

The proposed SNN is utilized to perform unsupervised classification by STDP learning scheme. By applying different patterns to input neurons, the output neurons generate patterns based on the weight update of connected synapses to them. One of the output neurons becomes a winner and reproduce one of the patterns in input due to the combination of connected synaptic weights. This happens when the weight vector of the winner output neuron is closer to one of the input pattern vector. For testing the functionality of the proposed ML-based SNN two simple pattern classification tasks have

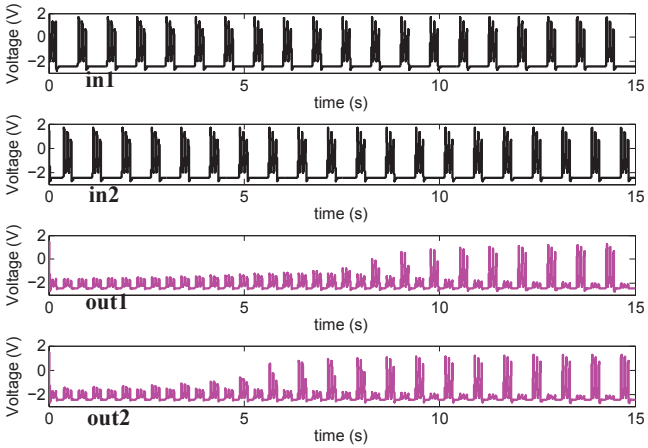

Fig. 7. The membrane voltage of the pre-synaptic (black curve) and post synaptic (purple curve) neurons for 2×2 network. The proposed network classifies the patterns successfully.

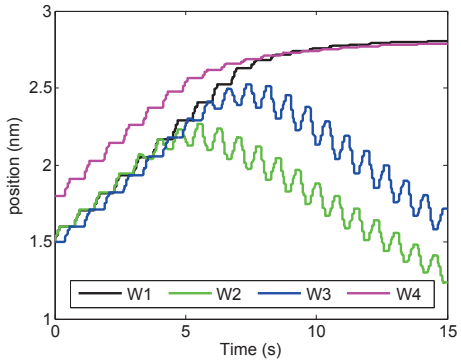

Fig. 8. The weight evolution of the memristive synapse for 2×2 network.

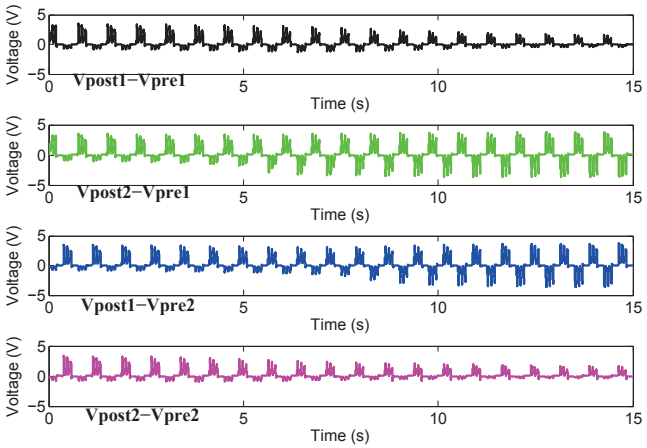

Fig. 9. The voltage over each memristive synapse that produce LTP or LTD phenomenons for 2×2 network.

been done. The first one is the 2×2 network that comprises of two input ML neurons $(\mathrm{in}_1, \mathrm{in}_2)$ and two output ML neurons $(\mathrm{out}_1, \mathrm{out}_2)$. These two layers are connected to each other by memristor synapses with random initial weights $(\mathrm{W}_1, \mathrm{W}_2, \mathrm{W}_3, \mathrm{W}_4)$. Each input neuron is connected to all

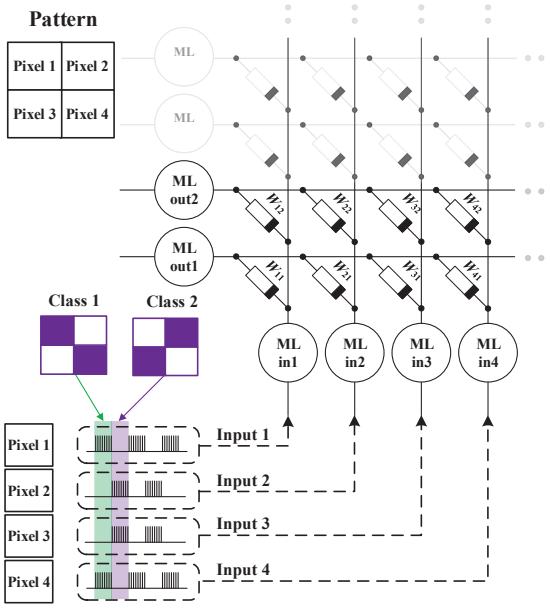

Fig. 10. 4×2 network architecture in memristive crossbar array for the proposed SNN. The input patterns for the proposed network are defined.

output neuron with one memristive synapse. This network is applied to classify between two pixel images with class 1 and 2. As it can be seen from the Fig. 6, two different input waves are applied to the input neurons. The input wave can be divided into several time frames and in each time frame one of the classes are applied. The input 1 and 2 are corresponding to the pixel 1 and 2 of the pattern, respectively. In the first time slot which is corresponding to class 1, the input 1 is spiking because pixel 1 is black and there is no spike for input 2 since the pixel 2 is white in this class. Subsequently, in the next time slot, class 2 of the two pixel image is applied as the input 1 is not spiking and input 2 is spiking.

The output for the proposed network with applied input waves are displayed in Fig. 7. It takes some times for post-synaptic ML neurons to follow one of the input patterns. The initial weight vector of each output neuron specifies the consumed time to follow the pattern and the pattern class to display due to its closeness to input patterns vector. Assuming the class 1 is assigned to the post-synaptic neuron 1, the weight of W_1 increases by LTP phenomenon as pre-synaptic neuron in_1 spikes before the post-synaptic neuron out_1. On the other hand, the weight of W_2 decreases due to the inactivity of out_2. The similar procedure is repeated for class 2 image. The memristive synapse weights and their behavior during STDP learning is displayed in Fig. 8. As it can be seen, W_1 and W_4 weights are increased and W_2 and W_3 are decreased. Also the voltage over each memristive synapse during STDP learning procedure and weight evolution is displayed in Fig. 9. The larger network, 4×2, is also tested with the proposed SNN. This network is displayed on memristive crossbar array in Fig. 10. The proposed network classifies 2 classes of the four pixel image. Two input patterns based on the classes are assigned to four input waves and applied to pre-synaptic neurons. These inputs are displayed in Fig. 11. The network is successfully performed the classification task and the output results are

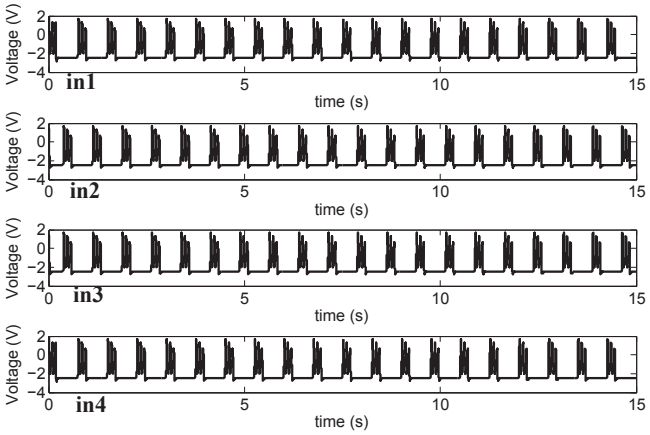

Fig. 11. The membrane voltages of the pre-synaptic neurons for 4×2 network.

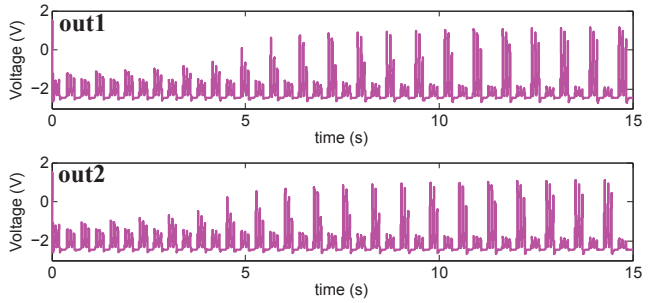

Fig. 12. The membrane voltage of the post-synaptic neurons for 4×2 network.

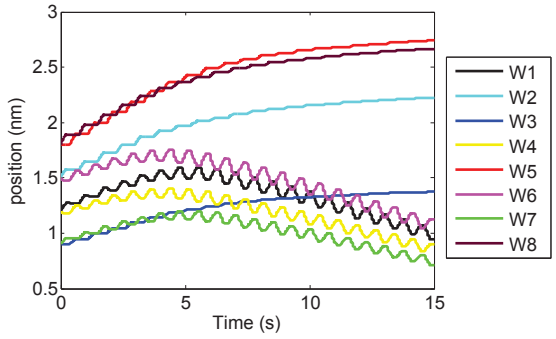

Fig. 13. The weights evolution of the memristive synapses for 4×2 network.

illustrated in Fig. 12 for both post-synaptic neurons. The weight evolution and behavior for each synapses are depicted in Fig. 13.

VII. Conclusion

This paper presented a memristive biological plausible spiking neural network with Morris-Lecar neuron model for pattern classification. The memristive implementation of ML neuron was explained and the potassium and calcium memristive channels behavior was investigated. The scaled model of the ML neuron was applied in a memristive SNN architecture and the STDP learning scheme was applied for pattern classification. Finally, two pattern classification examples was tested successfully with the proposed network as a proof of concept.

References

[1] S. B. Furber, S. Temple, and A. D, Brown, *"High performance computing for systems of spiking neurons,"* in Proc. AISB06 Workshop GC5: Archit. Brain Mind, vol. 2, pp. 29-36, 2006.

[2] M. J. Pearson, A. G. Pipe, B. Mitchinson, K. Gurney, C. Melhuish, I. Gilhespy, and M. Nibouche, *"Implementing spiking neural networks for real-time signal processing and control applications: A model-validated FPGA approach,"* IEEE Transactions on Neural Network, vol. 18, no. 5, pp. 1472-1487, 2007.

[3] W. Gerstner, and W. M, Kistler, *"Spiking Neuron Models: Single Neurons, Populations, Plasticity,"* Cambridge University Press, 2002.

[4] A. L. Hudgkin and A. F. Huxley, *"A quantitative description of membrane current and its application to conduction and excitation in nerve",* Journal of physiology, vol. 177, pp. 500-544, 1952.

[5] R. FitzHugh, *"Impulses and physiological states in theoretical models of nerve membrane",* Biophys. Journal, vol. 1, no. 6, pp. 445-466, 1961.

[6] J. Nagumo, S. Arimoto, and S. Yoshizawa *"An active pulse transmission line simulating nerve axon",* Proc. Inst. Radio Eng., vol. 50, no. 10, pp. 2061-2070, 1962.

[7] C. Morris and H. Lecar, *"A voltage oscillations in the barnacle giant musclefiber",* Biophys. Journal, vol. 35, pp. 193-213, 1981.

[8] E. M, Izhikevic, *"Resonant-and-fire neurons",* Neural Network, vol. 14, no. 6, pp. 883-894, 2001.

[9] J Toulboul, and R. Brette, *"Dynamics and bifurcations of the adaptive exponential integrate-and-fire mode",* Biological Cybernetics, vol. 99, no. 45, pp. 319-334, 2008.

[10] M. P, Sah H. Kim, A. Eroglue, and L. Chua, *"Memristive model of the barnacle giant muscle fibers,"*, International Journal of Bifurcation and Chaos, vol. 26, no. 1, pp. 1630001, 2016.

[11] G. Indiveri, B. Linares-Barranco, R. Legenstein, G. Deligeorgis, and T. Prodromakis, *"Integration of nanoscale memristor synapses in neuromorphic computing architectures,"*, Nanotechnology, vol. 24, no. 38, pp. 384010, 2013.

[12] K. D. Cantley, A. S. Subramaniam, H. J. Stiegler, and R. A. Chapman, *"Neural leraning circuits utilizing nano-crystaline silicon transistors and memristors,"* IEEE Transactions on Neural Network, vol. 23, no. 4, pp. 563-573, 2012.

[13] D. B. Strukov, G. S. Snider, D. R. Stewart, and R. S. Williams, *"The Missing Memristor Found,"* Nature, vol. 453, pp. 80-83, 2008.

[14] L. O. Chua, *"Memristor: the missing circuit element,"* IEEE Transactions on Circuit Theory, vol. 18, no. 5, pp. 507-519, 1971.

[15] Y. Ho, G. M. Huang, and P. Li, *"Nonvolatile memristor memory: Device characteristics and design implications,"* IEEE International Conference on Computer-Aided Design, pp. 485-490, 2009.

[16] M. Teimoory, A. Amirsoleimani, J. Shamsi, A. Ahmadi, S. Alirezaei and M. Ahmadi, *"Optimized implementation of memristor-based full adder by material implication logic,"* Electronics, Circuits and Systems (ICECS), 2014 21st IEEE International Conference on , pp. 562-565, 2014.

[17] M. Teimoory, A. Amirsoleimani, A. Ahmadi, S. Alirezaei, S. Salimpour and M. Ahmadi, *"Memristor-based linear feedback shift register based on material implication logic,"* Circuit Theory and Design (ECCTD), 2015 European Conference on, pp. 1-4, 2015.

[18] T. Serrano-Gotarredona, T. Masquelier, T. Prodromakis, G. Indiveri and B. Linares-Barranco, *"STDP and STDP variations with memristors for spiking neuromorphic learning systems",* Frontiers in neuroscince, vol. 7, 2013.

[19] A. Amirsoleimani, M. Ahmadi and M. Ahmadi, *"Brain-inspired pattern classification with memristive neural network using the Hodgkin-Huxley neuron,"* Electronics, Circuits and Systems (ICECS), 2016 IEEE Conference on, pp. 81-84, 2016.

[20] Z. Biolek, D. Biolek, and V. Biolkov, *"SPICE model of memristor with nonlinear dopant drift,"* Radioengineering, vol. 18, no. 2, pp. 210-214, 2009.